

Deep Generalized Convolutional Sum-Product Networks for Probabilistic Image Representations

Jos van de Wolfshaar^{1,2}, Andrzej Pronobis^{1,3}

¹KTH Royal Institute of Technology, Stockholm, Sweden

²MessageBird, Amsterdam, The Netherlands

³University of Washington, Seattle, WA, USA

jos.vandewolfshaar@gmail.com, pronobis@cs.washington.edu

Abstract

Sum-Product Networks (SPNs) are hierarchical, probabilistic graphical models capable of fast and exact inference that can be trained directly from high-dimensional, noisy data. Traditionally, SPNs struggle with capturing relationships in complex spatial data such as images. To this end, we introduce Deep Generalized Convolutional Sum-Product Networks (DGC-SPNs), which encode spatial features through products and sums with scopes corresponding to local receptive fields. As opposed to existing convolutional SPNs, DGC-SPNs allow for overlapping convolution patches through a novel parameterization of dilation and strides, resulting in significantly improved feature coverage and feature resolution. DGC-SPNs substantially outperform other convolutional and non-convolutional SPN approaches across several visual datasets and for both generative and discriminative tasks, including image completion and image classification. In addition, we demonstrate a modification to hard EM learning that further improves the generative performance of DGC-SPNs. While fully probabilistic and versatile, our model is scalable and straightforward to apply in practical applications in place of traditional deep models. Our implementation is tensorized, employs efficient GPU-accelerated optimization techniques, and is available as part of an open-source library based on TensorFlow.

Introduction

Sum-Product Networks (Poon and Domingos 2011) are deep probabilistic graphical models (PGM) (Koller, Friedman, and Bach 2009) designed with computational efficiency in mind. They allow for exact and efficient marginal, conditional, joint and MPE inference queries and naturally deal with missing data. SPNs can be seen as a special type of deep neural networks that can be trained using the techniques commonly used in deep learning such as adaptive gradient descent or dropout (Peharz et al. 2019), as well as other techniques used for PGMs (Zhao, Poupart, and Gordon 2016; Rashwan, Poupart, and Zhitang 2018). Due to their probabilistic interpretation, SPNs excel in domains with incomplete or noisy data, such as image classification with missing pixels or robotics (Peharz et al. 2019; Zheng, Pronobis, and Rao 2018).

Traditional convolutional neural networks (CNN) lack a probabilistic interpretation. In contrast, SPNs can perform

a wide range of probabilistic inferences efficiently through a single forward and backward pass. As a result, they are applicable to a wide range of both discriminative and generative tasks using a single architecture, including novelty detection, classification, data completion and generation (Poon and Domingos 2011; Gens and Domingos 2012; Zheng, Pronobis, and Rao 2018). Unlike neural networks, *valid* SPNs propagate exact probabilities, but are limited to using only products or sums with non-negative weights and subject to certain connectivity restrictions. These restrictions present a nontrivial challenge when designing convolutional SPNs.

In this work, we propose Deep Generalized Convolutional Sum-Product Networks (DGC-SPNs) that combine the probabilistic properties of SPNs with the ability to capture spatial relationships in a way similar to convolutional neural networks (CNNs). DGC-SPNs are deep, layered models that exploit the inherent structure of image data and hierarchically capture spatial relations through products and weighted sums with local receptive fields. We introduce a novel parameterization of strides, dilation rates and connectivity for convolutional operations in product layers that makes DGC-SPNs more general than existing approaches to convolutional SPNs (Sharir et al. 2016; Butz et al. 2019). Unlike other architectures, DGC-SPNs employ overlapping patches in product layers, avoiding the loss of feature resolution and coverage, while at the same time preserving the constraints that guarantee validity. We demonstrate that this translates to a significant improvement in performance for both generative as well as discriminative tasks, such as image completion and image classification. Finally, we analyze the behavior of generative learning with hard EM and propose to use unweighted sum inputs for MPE path selection. DGC-SPNs trained with this modified hard EM procedure yield even stronger improvements over existing methods for generative tasks.

Our main contributions are (i) the introduction of a novel convolutional SPN architecture, (ii) a comprehensive range of experiments with SPNs on image data where our DGC-SPNs substantially outperform other SPN models and (iii) a modified algorithm for hard EM learning of SPNs. Our model leverages the efficiency of the modern GPU-

accelerated TensorFlow framework (Abadi et al. 2015). Our code is part of a generic TensorFlow-based SPN library¹, which enables the application of a variety of learning algorithms (e.g. EM and gradient descent with adaptive learning rates), regularization methods and loss functions (Pronobis, Ranganath, and Rao 2017).

The paper is structured as follows: the next section introduces the theoretical background for SPNs. Then, we discuss related research on SPN-based approaches for visual tasks. We then elaborate on the workings of DGC-SPNs. In addition, we provide a modification to hard EM that significantly improves performance for image completion. Finally, we compare the performance of DGC-SPNs against other SPN approaches for both generative as well as discriminative tasks.

Background

A Sum-Product Network $S(\mathbf{x})$ represents a joint probability distribution over a set of random variables \mathbf{X} . An example of a simple SPN is given in Figure 1. An SPN is a rooted directed acyclic graph where the root node computes the unnormalized probability $S(\mathbf{x})$ of a distribution at $\mathbf{x} \in \mathbf{X}$. The leaves of an SPN correspond to individual random variables X_i . In the discrete case, they are typically represented as Bernoulli variables, while Gaussian distributions are often used for continuous inputs. In between the leaves and the root, an SPN contains weighted sum and product operations. The weighted sum nodes have non-negative weights and can be interpreted as probabilistic mixture models over subsets of variables, while products compute joint probabilities by multiplying input values and can be seen as features. The output of a sum node s_j is given by $S_{s_j}(\mathbf{x}) = \sum_{i \in \text{ch}(s_j)} w_{ji} C_i$ where C_i is the value of the i -th child and $\text{ch}(s_j)$ is the set of children of s_j . The output of a product node p_j is given by $S_{p_j}(\mathbf{x}) = \prod_{i \in \text{ch}(p_j)} C_i$.

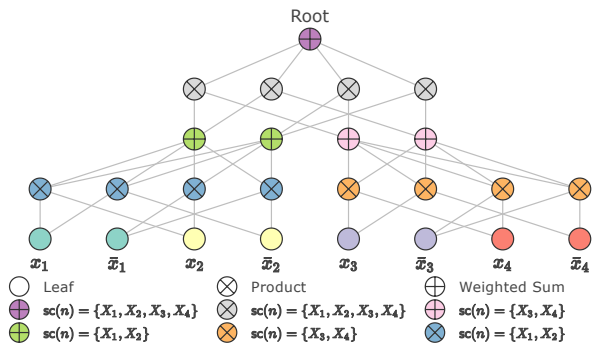


Figure 1: An example of an SPN with 4 discrete binary variables.

Following (Poon and Domingos 2011), we define the following concepts related to SPNs:

¹<https://www.libspn.org>

Definition 1 (Scope). The scope of a node n , denoted $\text{sc}(n)$, is the set of variables that are descendants of n .

In other words, the scope of a node is the union of the scopes of its children. Typically, leaf nodes have a *singular* scope containing a single variable X_i .

Definition 2 (Validity). An SPN is valid if it correctly computes the unnormalized probability for all evidence e where $e \subseteq \mathbf{X}$.

A sufficient set of conditions that ensure validity consists of *completeness* and *decomposability*:

Definition 3 (Completeness). An SPN is complete if all children of a sum node have identical scopes.

Definition 4 (Decomposability). An SPN is decomposable if all children of the same product node have pairwise disjoint scopes.

Evaluating an SPN without any evidence gives the partition function $Z_S = \sum_{\mathbf{x} \in \mathbf{X}} S(\mathbf{x})$ which can be used as the normalization constant for computing the probability of \mathbf{x} : $P(\mathbf{x}) = S(\mathbf{x})/Z_S$. The constant Z_S is computed by setting the output of each leaf node to 1. For a Bernoulli variable X_i , both indicators x_i and \bar{x}_i are set to 1. If all X_i are continuous and represented as multiple Gaussian components per variable, then all of the components corresponding to X_i are set to 1. It has been proven that $Z_S = 1$ for a *normalized* SPN, where the weights of each sum node add up to one. A normalized SPN computes a probability with a single upward pass: $S(\mathbf{x}) = P(\mathbf{x})$ and correctly models a probability density function or a probability mass function (Peharz 2015).

Parameter Learning for SPNs

For discriminative tasks, SPNs can be trained with traditional gradient descent techniques used in deep learning, such as SGD or Adam (Kingma and Ba 2014). For generative tasks, EM is often the algorithm of choice.

In practice, SPNs are often trained with *hard* EM, which overcomes the issue of diminishing gradients present in deep models. Hard EM is accomplished by accumulating the number of times a weight was part of an MPE path. The MPE path can be found by following the child with maximum weighted probability at sum nodes and splitting the path at products, starting from the root. For each sum node, the final weights are determined by normalizing the path accumulators c_i , i.e. $w_i = c_i / \sum_j c_j$ where we sum over all accumulators of the corresponding sum. Based on our experiments, we propose a small modification to online hard EM that significantly improves the generative abilities of our SPNs.

Related Work on Visual Tasks with SPNs

There have been numerous attempts to apply various SPN architectures to both discriminative and generative visual tasks. In (Poon and Domingos 2011), SPNs were used for image completion on several datasets. The SPNs in (Poon and Domingos 2011) were built so that each rectangular region is recursively split into all possible vertical and horizontal rectangular subregions (APVAHRS). The smallest

region in the APVAHRS architecture consists of one pixel. The APVAHRS architecture has also been trained with the Extended-Baum Welch (EBW) algorithm to perform image classification (Rashwan, Poupert, and Zhitang 2018).

Closely related to our work are Convolutional Arithmetic Circuits (ConvACs) (Sharir et al. 2016) and Deep Convolutional Sum-Product Networks (Butz et al. 2019). ConvACs can be viewed as convolutional SPNs. Both ConvACs and DCSPNs ensure decomposability of products by using non-overlapping image patches for the convolutions, by which they effectively downsample the feature resolution and fail to cover all possible image patches. In contrast, DGC-SPNs employ a more general approach to convolutions that allow for significantly improved feature coverage and resolution. A hybrid architecture consisting of neural convolutional layers and an SPN was used for image classification in (Hartmann 2014). However, this yields an architecture that is not fully probabilistic, thereby lacking the ability to perform probabilistic inferences all the way down to the inputs of the model.

Apart from spatial SPNs, other works for visual tasks with SPNs consider randomly structured SPNs (Peharz et al. 2019), an SVD-based structure learning algorithm (Adel, Balduzzi, and Ghodsi 2015), a structure learning algorithm based on clustering of variables (Dennis and Ventura 2012), or a structure learning algorithm based on both correlation matrices and clustering (Jaini, Ghose, and Poupert 2018). Rather than using random or learned structures, DGC-SPNs impose a spatial prior on the structure that adequately captures the inherent spatial relations present in image data.

We show that DGC-SPNs yield substantial performance improvements over the aforementioned SPN approaches in our experiments.

Deep Generalized Convolutional SPNs

Deep Generalized Convolutional Sum-Product Networks (DGC-SPNs) are a new type of convolutional SPN. An example of a DGC-SPN is depicted in Figure 2. DGC-SPNs consist of products or weighted sums that combine their inputs locally in a way similar to CNNs. Since our implementation is tensorized, we first explain the interpretation of each tensor dimension. DGC-SPN layers are represented as tensors with one dimension for the samples in the batch, an arbitrary number of spatial dimensions (e.g. 2 for image input), and a dimension for channels. From hereon, we omit the batch dimension and discuss DGC-SPNs for a single sample for simplicity. For image data, a tensor $X \in \mathbb{R}^{H \times W \times C}$ with width W , height H and number of channels C (e.g. RGB channels for color images) contains a *cell* at a single location (i, j) indexed on the spatial axes, denoted $X[i, j, :]$, where \cdot is used to refer to all elements along the corresponding axis. For 1D spatial data, a cell is indexed by $X[i, :]$. An SPN *node* in a DGC-SPN is either a sum or a product at a particular channel and cell and can be thought of as the elementary component of a tensor, indexed by $X[i, j, k]$ for 2D data or $X[i, k]$ for 1D data. Nodes are stacked along the channel axis to form cells, while cells are stacked along the spatial axes to form layers. Sum layers and product layers are stacked in alternating fashion to form

a deep network. Figure 2 provides a visual explanation of layers, channels, cells and nodes.

Scopes in Spatial SPNs

For spatial SPNs, the scopes have a clear relation to the tensor dimensions mentioned above. If we consider a single cell at the input tensor, we find multiple channels that cover the same variable X_i . These channels can be e.g. different Gaussian components in case of continuous data or different indicators in case of discrete data. Since the channels within a cell cover the same variable, they have the same singleton scope $\{X_i\}$. In other words, scopes *within a cell* of the input tensor are *homogeneous*. In contrast, for image data, different cells at the input correspond to different pixels. If we take any *pair of cells*, we can say that the scopes of these cells are *heterogeneous*.

By ensuring that sum layers and product layers preserve within-cell homogeneity, across-cell heterogeneity, completeness and decomposability, we can derive valid convolutional SPN architectures. We now elaborate on how to implement and parameterize such spatial layers.

Spatial Sum Layers

Completeness applies to sum nodes. A sum is complete if it has children with *identical scopes*. The within-cell homogeneity and across-cell heterogeneity dictate that a sum’s children should only be connected to a single input channel. We can add multiple single-cell sums above each input cell to form a layer of sums with the same number of cells as the input layer leading to an arbitrary amount of output channels. Hence, the spatial layout of the scopes remains unchanged.

Spatial Product Layers

Products are decomposable if they are connected to children with pairwise disjoint scopes. Since spatial SPN layers have within-cell homogeneity and across-cell heterogeneity, products can have children from at most one channel per cell, but cover two or more input cells. At the input layer, it is trivial to see that neighboring cells are not only heterogeneous, but also pairwise disjoint. Hence, the products on top of an input layer can join scopes by taking small patches of several cells while selecting only one input channel per cell.

Products as Convolutions SPNs are implemented to propagate log-probabilities to avoid underflow. Hence, the local patches of products become local patches of sums with one-hot weights per cell. We refer to this interpretation as a convolutional log-product (CLP). Figure 2 displays CLPs with one-hot weights highlighted by the blue and red lines. A red line indicates that the product is connected to the top channel of the input cell, while a blue line indicates that the product is connected to the bottom channel of the input cell.

In general, there are C^t combinations of child nodes per patch where C is the number of input channels and t is the number of cells under a patch. To limit the number of products, one can take a random subset of combinations. Depth-wise convolutions are a special case of CLP where the number of output channels equals the number of input channels,

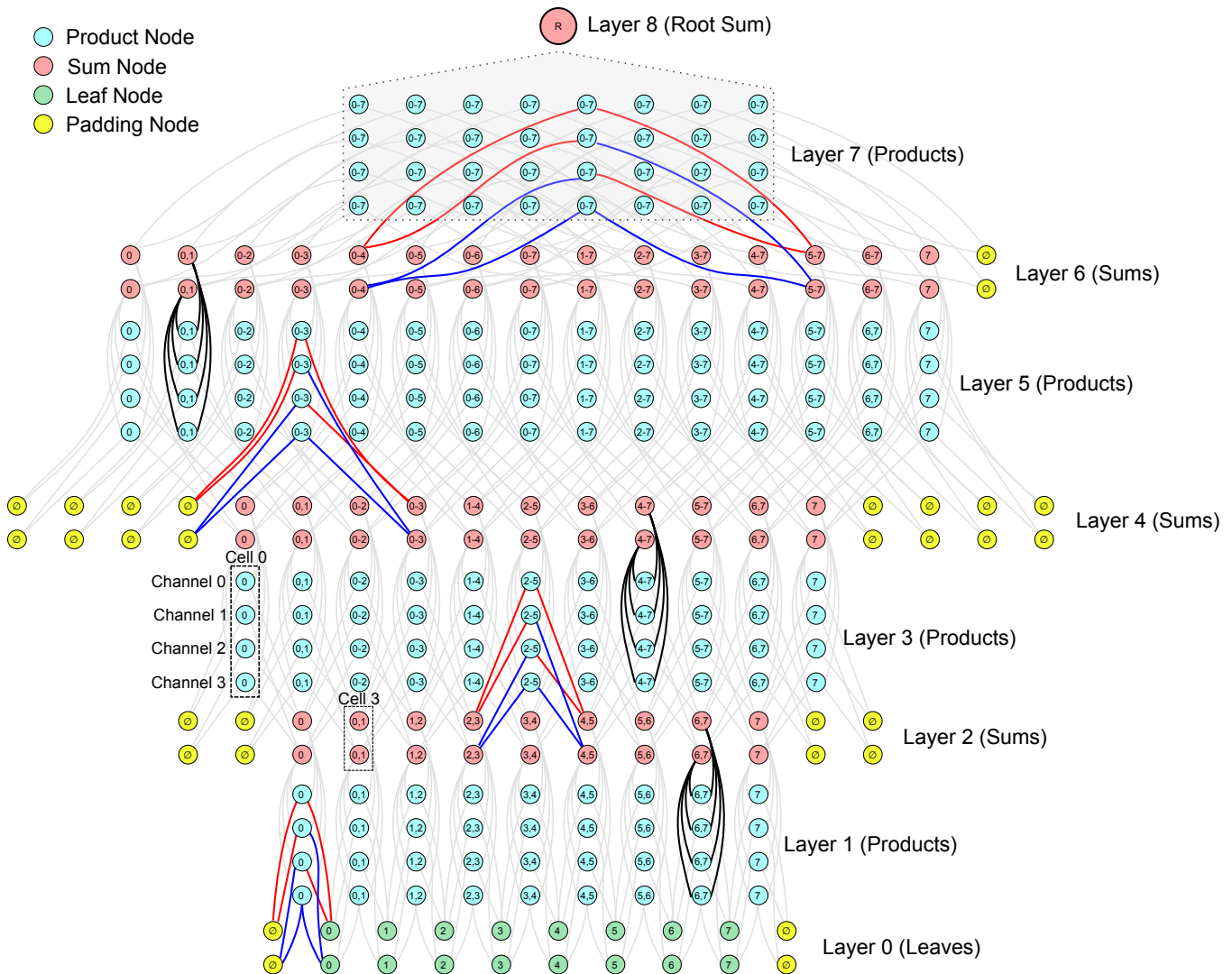


Figure 2: A simplified illustration of a DGC-SPN in 1D. Node types are indicated by different colors. The nodes of a single cell share the same scope. Layer 0 contains leaf distributions, where the channel corresponds to the indicator for discrete variables or the distribution component (e.g. Gaussian) for continuous variables. Every new layer of products doubles the dilation rate, starting at a rate of 1. For each layer, connections for only one cell are highlighted to avoid clutter. The scopes are indicated by the numbers within each node. Padding nodes have a fixed probability of 1 (or 0 in log-space). All children of the root node R have a scope that contains all input variables.

which is also referred to as sum-pooling (Sharir et al. 2016; Butz et al. 2019). However, CLPs with one-hot cells in their kernels offer a more general approach.

Generalized Convolutional Log Products Existing approaches to convolutional SPNs (Sharir et al. 2016; Butz et al. 2019) use non-overlapping patches for their products. Hence, neighboring cells in the output of such layers are not only heterogeneous, but also pairwise disjoint. However, non-overlapping patches require strides larger than 1, thus skipping many combinations of input cells, yielding suboptimal feature coverage. In fact, this becomes visibly apparent in patch-wise artifacts in image completions (Butz et al. 2019).

To overcome these limitations, DGC-SPNs use generalized convolutional log-products (GCLPs). A GCLP is obtained by (i) ‘full’ padding (Dumoulin and Visin 2016), (ii) strides as small as 1, and (iii) exponentially increasing dilation rates. A dilated kernel with a dilation rate of d takes in cells that are d positions apart. The first GCLP in Figure 2 takes layer 0 as input and yields layer 1 as output. Its kernels use a dilation rate of 1. We see that the convolutional patches overlap as a consequence of unit strides. Hence, neighboring cells in layer 1 are heterogeneous, but not pairwise disjoint. This forbids us from applying another convolution with a dilation rate of 1. Instead, we exponentially increase the dilation rate to obtain a spacing in

our kernels that ‘skips’ the input cells that would otherwise yield non-disjoint children. The exponentially increasing dilation rates yield patches covering pairwise disjoint scopes. Hence, GCLPs exhibit significantly improved feature coverage while preserving decomposability.

Full padding is required to make sure that any cell in a layer can be assigned to a disjoint group of cells from the same layer so that a parent of this group has a scope that contains all variables. Otherwise, for the DGC-SPN in Figure 2, there would be no cells with scopes of $\{0\}$ or $\{7\}$ after the first GCLP to be combined with $\{1, 2\}$, $\{3, 4\}$ and $\{5, 6\}$ to obtain a scope with all variables. After $\lceil \log_2(w) \rceil$ GCLPs with kernel size 2 (where w is the width of the input), we obtain cells that can be combined with at most one other cell to form an output layer with cells that have scopes that include all variables.

For readability, the above explanation of DGC-SPNs focusses on 1 spatial dimension and kernel sizes of 2 for all GCLPs. Nevertheless, our architecture generalizes to any number of spatial dimensions and kernel sizes that vary per layer as shown in our experiments.²

Experiments

We evaluated the generative and discriminative capabilities of DGC-SPNs on different visual tasks: image completion and image classification.

Table 1: Default settings for generative and discriminative experiments. In some cases the parameters vary depending on the layer. For example, $[64]^3[128]^2$ means that the value is 64 for the first 3 layers and 128 for the last 2. We use D to indicate the complete depth of the network.

Name	Generative	Discriminative
Kernel size CLP	$[2 \times 2]^D$	$[2 \times 2]^6$
Sums per scope/cell	$[16]^D$	$[64]^3[128]^2$
Strides	$[1]^D$	$[2]^2[1]^4$
Full padding	$[\checkmark]^D$	$[\times]^2[\checkmark]^4$
Depthwise CLP	$[\times]^1[\checkmark]^{D-1}$	$[\checkmark]^D$
Leaf distribution	$\mathcal{N}(\mu_i, 1)$	$\mathcal{N}(\mu_i, 1)$
Components per pixel	4	32
Leaf means init	$\mu_i = q(i, X)$	Equidistant
Additive smoothing	$10^{-2}/ w $	\times
Learning algorithm	Hard EM	Adam
p_{PD}	–	0.2
p_{ID}	–	0.2
Normalize X	\checkmark	\checkmark
Batch size	128	64
Epochs	25	400

Experimental Setup

We discuss generative and discriminative setups in separate sections and begin each with a detailed description of the

²In case of varying kernel sizes, the GCLP dilation rates must equal the product of all preceding GCLP kernel sizes rather than increase exponentially.

datasets used in the experiments. A detailed specification of the structural parameters and other hyperparameters used can be found in Table 1.

Generative Learning We assessed generative capabilities of DGC-SPNs through image completion. We used the Caltech dataset (Fei-Fei, Fergus, and Perona 2004) and the Olivetti faces dataset (Samaria and Harter 1994). We employed the same 64×64 crops and the same train and test splits as used in (Poon and Domingos 2011) to ensure a fair comparison. In addition, we used the MNIST dataset (Lecun et al. 1998) which contains images of handwritten digits and the Fashion MNIST (Xiao, Rasul, and Vollgraf 2017) with images of cloth. For both MNIST and Fashion MNIST we used the default train and test splits. In all experiments, pixels were normalized sample-wise by subtracting the mean and dividing by the standard deviation for each image.

To build DGC-SPNs, we used a Gaussian leaf layer followed by a GCLP layer. We used depthwise convolutions for all but the first GCLP. The first GCLP computed all possible combinations of children under each patch. We alternated between sum layers and GCLPs until we arrived at the final GCLP layer that consists of cells with all variables in their scopes.³

We trained our generative SPNs with online hard EM. Although hard EM formally requires MPE inference in the forward pass, we followed the suggested modification in (Poon and Domingos 2011) to use marginal inference in the forward pass instead. We broke ties for sum children by choosing a random child among the ones with maximum weighted probabilities. We initialized the MPE path accumulators c_i to zero. The weights were obtained by normalizing the MPE path accumulators through

$$w_i = \frac{c_i + \varepsilon}{\sum_j c_j + \varepsilon}, \quad (1)$$

where we used additive smoothing dependent on the number of weights per sum: $\varepsilon = 10^{-2}/|w|$.

The mean of the i -th Gaussian component of a pixel was initialized with the mean of the i -th quantile split of the pixel based on the train data (Poon and Domingos 2011). We abbreviate this type of initialization with $\mu_i = q(i, X)$ in Table 1. The means and variances of the leaves were not trained.

We performed image completion by computing the marginal posterior probability at the Gaussian leaves through partial derivatives (Darwiche 2003). The partial derivatives were used as coefficients to linearly combine the modes of the leaf distributions, resulting in the actual predicted completion values (Poon and Domingos 2011).

Discriminative Learning We assessed the discriminative abilities of DGC-SPNs with the task of image classification on the MNIST (Lecun et al. 1998) and Fashion MNIST datasets (Xiao, Rasul, and Vollgraf 2017), again with their

³Given that the Olivetti dataset is small, we used SPNs with fewer trainable parameters for this dataset. In that case, we used a depthwise GCLP only for the first layer and we used sum layers with 2 channels, which were each followed by GCLPs which consider all possible combinations of children.

default train and test splits. We performed sample-wise normalization in the same way as the generative case.

To build DGC-SPNs, we used a Gaussian leaf layer followed by a GCLP. As opposed to the generative case, we first performed two non-overlapping GCLPs without padding and used GCLPs with overlapping patches thereafter. We alternated between sum layers and GCLPs until we arrived at the final GCLP layer that consists of cells that have scopes with all variables. Several other SPN approaches, including (Gens and Domingos 2012; Hartmann 2014), require sub-SPNs *per class* after which the class-specific SPNs are combined by a single sum node at the root of the SPN. Consequently, these SPN architectures scale poorly when the number of classes is large. In contrast, our DGC-SPNs use only a single stack of product and sum layers which is shared for all classes followed by a layer of K sums (where K is the number of classes) and a root node. Hence, our DGC-SPNs are scalable to datasets with potentially thousands of classes.

We used the Adam optimizer (Kingma and Ba 2014) with default settings. We parameterized the sums with log-space accumulators (Peharz et al. 2019), denoted $c'_i = \log(c_i)$ as opposed to linear-space accumulators c_i . We normalized these accumulators c'_i through

$$w'_i = \log\left(\frac{c_i}{\sum_j c_j}\right) = c'_i - \log\left(\sum_j \exp(c'_j)\right), \quad (2)$$

so that we obtained log-space weights w'_i . The means of the Gaussian components at the leaf layer were initialized with equidistant intervals in the range of $[-1.5, 1.5]$, while their variances were initialized to 1. The means of the leaves were trained, whereas their variances were fixed during training.

For regularization, we applied product dropout (PD) (Peharz et al. 2019) by randomly setting products to zero probability with a rate of $p_{PD} = 0.2$ throughout the entire network. Finally, we applied input dropout (ID) by setting the components of a variable X_i to 1 at random with a rate of $p_{ID} = 0.2$ (Peharz et al. 2019), as if the dropped out variables were excluded from the evidence.

Results

Below, we present the results of our experiments with both generative and discriminative learning.

Generative Learning Table 2 shows the results for generative unsupervised learning. We tasked the models with recreating half of an image based on its other half, an extremely difficult problem for a deep architecture. We masked either the left or the bottom half of the images. The performance was assessed based on the mean squared error (MSE) between pixel values of the completions versus the original images. Pixels were scaled to the range of $[0, 255]$ when computing the MSEs.

In our experiments with vanilla hard EM, we observed that the variance of log probabilities of sum inputs decrease exponentially with the depth of the SPN (see Figure 3). This

⁴MSEs taken from (Butz et al. 2019) were doubled based on a bug in their code: github.com/jhonatanoliveira/dcpsns/issues/1.

Table 2: Unsupervised image completion. The uppermost results for Olivetti and Caltech are taken from (Poon and Domingos 2011). The DCSPN results for Olivetti are taken from (Butz et al. 2019). The ClusterVars architecture is the learned structure from (Dennis and Ventura 2012). We trained DGC-SPNs with and without unweighted sum inputs (USI). The values correspond to the mean squared errors of completion vs. original pixel values for the occluded part of the image averaged over 5 independent runs.

Dataset	Method	Bottom	Left
Olivetti	APVAHRS	918	942
Olivetti	ClusterVars	820	814
Olivetti	DCSPN ⁴	1006	910
Olivetti	DGC-SPN	804	847
Olivetti	DGC-SPN + USI	724	801
Caltech	APVAHRS	3270	3551
Caltech	DGC-SPN	3216	3161
Caltech	DGC-SPN + USI	2801	2722
MNIST	DGC-SPN	3767	3102
MNIST	DGC-SPN + USI	2996	2476
FMNIST	DGC-SPN	2870	2268
FMNIST	DGC-SPN + USI	2223	1637

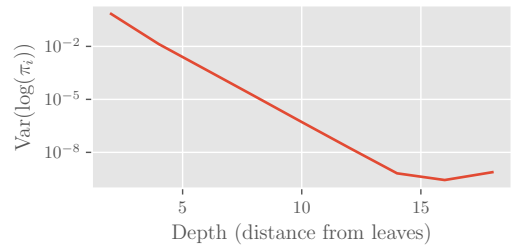


Figure 3: Average variance of the log probability of sum child $\log(\pi_i)$ versus layer depth for binarized MNIST data. The SPN uses 2 children and 4 sums per scope with a random structure and random weights. Note that we use a log-scale axis for the variance of the log probabilities. The graph shows an exponentially decreasing variance, except for a depth greater than 14, which might be explained by numerical precision errors.

poses a strong bias towards the winning sum child in deeper layers, since the weights themselves vary much stronger than the inputs of the sums. We hypothesized that this effect might be detrimental to the learning process. Hence, to eliminate the influence of weights for the selection of the winning sum child, we trained SPNs with EM using unweighted sum inputs for path determination (Kalra et al. 2018).

For all but one other result from the literature, DGC-SPNs trained with vanilla hard EM outperformed related SPN approaches for both bottom-occluded and left-occluded images. The sole exception is the ClusterVars architecture (Dennis and Ventura 2012) that performed slightly better for left-completion for the Olivetti dataset compared to the DGC-SPN trained without USI, while the DGC-SPNs without USI still performed better for bottom-occluded images.

Table 3: Results of discriminative experiments on multiple datasets. The accuracies are averaged over 5 independent runs.

Dataset	Algorithm	Architecture	Authors	Accuracy
MNIST	EBW	APVAHRS	(Rashwan, Poupart, and Zhitang 2018)	95.07%
MNIST	DSPN-SVD	Learned	(Adel, Balduzzi, and Ghodsi 2015)	97.34%
MNIST	Prometheus	Learned	(Jaini, Ghose, and Poupart 2018)	98.37%
MNIST	SGD	CNN + SPN	(Hartmann 2014)	98.34%
MNIST	Adam	RAT-SPN	(Peharz et al. 2019)	98.19%
MNIST	Adam	DGC-SPN	Ours	98.66%
FMNIST	Adam	RAT-SPN	(Peharz et al. 2019)	89.52%
FMNIST	Adam	DGC-SPN	Ours	90.74%

Hard EM with unweighted sum inputs (USI in Table 2) clearly improves the completion MSEs. Although the use of unweighted sum inputs were mentioned in the supplementary material of (Kalra et al. 2018), it contained no comparison against performance with weighted sum inputs, nor did it provide an intuition on why this improves generative performance. We suggest the improvements observed here can be attributed to the fact that exponentially decreasing variances cause strong biases in path selection, which is mitigated through eliminating the effect of weights in path selection by using unweighted sum inputs instead. DGC-SPNs trained with this modification outperform the related approaches consistently with an even greater margin.



Figure 4: Completions for left-occluded test images from the Olivetti dataset. We alternate rows of original images and completions with DGC-SPNs. The image shows the full test set, so it fairly displays the ability of DGC-SPNs to perform such completions.

Figure 4 shows completions for left-occluded images from the Olivetti dataset for one of our experiments with unweighted sum inputs. The figure includes all images in

the test set, illustrating the ability of DGC-SPNs to perform completions without selection bias.

Discriminative Learning Table 3 provides an overview of image classification results where we compare test classification accuracies of DGC-SPNs against related work with SPNs. DGC-SPNs outperformed all other approaches for both the MNIST and Fashion MNIST datasets.

Conclusions

This paper introduced DGC-SPNs, a novel, scalable, deep convolutional architecture for representing spatial and image data applicable to both generative and discriminative tasks. DGC-SPNs are the most general realization of convolutional SPNs to date, allowing for overlapping convolution patches without breaking validity thanks to a unique parameterization of strides and dilations. This translates to a significant improvement in performance. In our experiments, DGC-SPNs offered state-of-the-art results compared to related SPN architectures on several visual tasks and datasets. In addition, our experiments provided an empirical motivation for the use of unweighted sum inputs for generative learning with hard EM and demonstrated substantial improvements over vanilla hard EM.

As opposed to CNNs, DGC-SPNs are fully probabilistic, naturally deal with missing inputs, and are capable of efficient joint, marginal, and conditional queries over complex, noisy data. Moreover, the proposed architecture is applicable to other spatial data beyond images and 2 dimensions. This makes it particularly suitable for domains that require reasoning with uncertainty, such as robotics.

In future work, we intend to further draw from the pool of ideas applied to CNNs. Moreover, by releasing an implementation based on the well established TensorFlow framework, we would like to encourage further development and application of spatial SPN architectures.

Acknowledgements

This work was supported by the Swedish Research Council (VR) project 2012-4907 SKAEENet. We would like to thank Avinash Raganath for his indispensable contributions to the LibSPN library and insightful discussions during the time we spent together at KTH. Last but not least, we would like to express our gratitude to Prof. Rajesh P. N. Rao for his unwavering support, encouragement, and invaluable advice.

References

- Abadi, M.; Agarwal, A.; Barham, P.; Brevdo, E.; Chen, Z.; Citro, C.; Corrado, G. S.; Davis, A.; Dean, J.; Devin, M.; Ghemawat, S.; Goodfellow, I.; Harp, A.; Irving, G.; Isard, M.; Jia, Y.; Jozefowicz, R.; Kaiser, L.; Kudlur, M.; Levenberg, J.; Mané, D.; Monga, R.; Moore, S.; Murray, D.; Olah, C.; Schuster, M.; Shlens, J.; Steiner, B.; Sutskever, I.; Talwar, K.; Tucker, P.; Vanhoucke, V.; Vasudevan, V.; Viégas, F.; Vinyals, O.; Warden, P.; Wattenberg, M.; Wicke, M.; Yu, Y.; and Zheng, X. 2015. TensorFlow: Large-scale machine learning on heterogeneous systems. Software available from tensorflow.org.
- Adel, T.; Balduzzi, D.; and Ghodsi, A. 2015. Learning the Structure of Sum-product Networks via an SVD-based Algorithm. In *Proceedings of the Thirty-First Conference on Uncertainty in Artificial Intelligence, UAI'15*, 32–41. Arlington, Virginia, United States: AUAI Press.
- Butz, C.; Oliveira, J.; dos Santos, A.; and Teixeira, A. 2019. Deep Convolutional Sum-Product Networks. In *Thirty-Third AAAI Conference on Artificial Intelligence (AAAI)*.
- Darwiche, A. 2003. A Differential Approach to Inference in Bayesian Networks. *J. ACM* 50(3):280–305.
- Dennis, A., and Ventura, D. 2012. Learning the architecture of sum-product networks using clustering on variables. In Pereira, F.; Burges, C. J. C.; Bottou, L.; and Weinberger, K. Q., eds., *Advances in Neural Information Processing Systems 25*. Curran Associates, Inc. 2033–2041.
- Dumoulin, V., and Visin, F. 2016. A Guide to Convolution Arithmetic for Deep Learning. *arXiv preprint arXiv:1603.07285*.
- Fei-Fei, L.; Fergus, R.; and Perona, P. 2004. Learning Generative Visual Models from Few Training Examples: An Incremental Bayesian Approach Tested on 101 Object Categories. In *2004 Conference on Computer Vision and Pattern Recognition Workshop*, 178–178.
- Gens, R., and Domingos, P. 2012. Discriminative Learning of Sum-Product Networks. In Pereira, F.; Burges, C. J. C.; Bottou, L.; and Weinberger, K. Q., eds., *Advances in Neural Information Processing Systems 25*. Curran Associates, Inc. 3239–3247.
- Hartmann, T. 2014. *Discriminative Convolutional Sum-Product Networks on GPU*. Ph.D. Dissertation, Rheinische Friedrich-Wilhelms-Universität Bonn.
- Jaini, P.; Ghose, A.; and Poupart, P. 2018. Prometheus : Directly Learning Acyclic Directed Graph Structures for Sum-Product Networks. In Kratochvíl, V., and Studený, M., eds., *Proceedings of the Ninth International Conference on Probabilistic Graphical Models*, volume 72 of *Proceedings of Machine Learning Research*, 181–192. Prague, Czech Republic: PMLR.
- Kalra, A.; Rashwan, A.; Hsu, W.-S.; Poupart, P.; Doshi, P.; and Trimonias, G. 2018. Online Structure Learning for Feed-Forward and Recurrent Sum-Product Networks. In Bengio, S.; Wallach, H.; Larochelle, H.; Grauman, K.; Cesa-Bianchi, N.; and Garnett, R., eds., *Advances in Neural Information Processing Systems 31*. Curran Associates, Inc. 6944–6954.
- Kingma, D. P., and Ba, J. 2014. Adam: A Method for Stochastic Optimization. *CoRR* abs/1412.6980.
- Koller, D.; Friedman, N.; and Bach, F. 2009. *Probabilistic Graphical Models: Principles and Techniques*. MIT press.
- Lecun, Y.; Bottou, L.; Bengio, Y.; and Haffner, P. 1998. Gradient-Based Learning Applied to Document Recognition. In *Proceedings of the IEEE*, 2278–2324.
- Peharz, R.; Vergari, A.; Stelzner, K.; Molina, A.; Shao, X.; Trapp, M.; Kersting, K.; and Ghahramani, Z. 2019. Random Sum-Product Networks: A Simple and Effective Approach to Probabilistic Deep Learning. In *Proceedings of the 35th Conference on Uncertainty in Artificial Intelligence*.
- Peharz, R. 2015. *Foundations of Sum-Product Networks for Probabilistic Modeling*. Ph.D. Dissertation, Graz University of Technology.
- Poon, H., and Domingos, P. 2011. Sum-Product Networks: A New Deep Architecture. In *Computer Vision Workshops (ICCV Workshops), 2011 IEEE International Conference on*, 689–690. IEEE.
- Pronobis, A.; Ranganath, A.; and Rao, R. P. 2017. LibSPN: A Library for Learning and Inference with Sum-Product Networks and TensorFlow. In *ICML 2017 Workshop on Principled Approaches to Deep Learning*.
- Rashwan, A.; Poupart, P.; and Zhitang, C. 2018. Discriminative Training of Sum-Product Networks by Extended Baum-Welch. In Kratochvíl, V., and Studený, M., eds., *Proceedings of the Ninth International Conference on Probabilistic Graphical Models*, volume 72 of *Proceedings of Machine Learning Research*, 356–367. Prague, Czech Republic: PMLR.
- Samaria, F. S., and Harter, A. C. 1994. Parameterisation of a Stochastic Model for Human Face Identification. In *Proceedings of 1994 IEEE Workshop on Applications of Computer Vision*, 138–142.
- Sharir, O.; Tamari, R.; Cohen, N.; and Shashua, A. 2016. Tensorial Mixture Models. *arXiv preprint arXiv:1610.04167*.
- Xiao, H.; Rasul, K.; and Vollgraf, R. 2017. Fashion-MNIST: a Novel Image Dataset for Benchmarking Machine Learning Algorithms.
- Zhao, H.; Poupart, P.; and Gordon, G. J. 2016. A Unified Approach for Learning the Parameters of Sum-Product Networks. In Lee, D. D.; Sugiyama, M.; Luxburg, U. V.; Guyon, I.; and Garnett, R., eds., *Advances in Neural Information Processing Systems 29*. Curran Associates, Inc. 433–441.
- Zheng, K.; Pronobis, A.; and Rao, R. P. N. 2018. Learning graph-structured sum-product networks for probabilistic semantic maps. In *Proceedings of the Thirty-Second AAAI Conference on Artificial Intelligence, (AAAI-18), the 30th innovative Applications of Artificial Intelligence (IAAI-18), and the 8th AAAI Symposium on Educational Advances in Artificial Intelligence (EAAI-18), New Orleans, Louisiana, USA, February 2-7, 2018*, 4547–4555.